JOURNAL of
MATERIALS and MECHATRONICS:A

e-ISSN 2717-8811
JournalMM, 2024, 5(2), 327-340
https://doi.org/10.55546/jmm.1584040

Araştırma Makalesi / Research Article

The Influence of B Content on the Microstructure and Hardness of in Situ Formed TiC-TiB_2 Reinforced Fe-Based Hardfacing Coatings

Bülent KILINÇ[1*]

[1*] Sakarya University of Applied Sciences, Machine and Metal Department, Vocational School of Arifiye, Sakarya, Türkiye, ORCID ID: https://orcid.org/0000-0003-4928-7148, bkilinc@subu.edu.tr

Geliş/ Received: 13.11.2024**;** **Revize/Revised:** 26.11.2024 **Kabul / Accepted:** 01.12.2024

ABSTRACT: In this study, Fe-Cr-Ti-(B, C) based hardfacing coatings with different ratios were produced on DIN St37 steel plate surface using tungsten inert gas (TIG) welding method. It was investigated how increasing boron content affects the morphology of in situ TiC-TiB_2 phases expected to form in situ in the coating. The effects of these changes in microstructure on the microhardness of the hardfacing coatings were also determined. X-ray analyses revealed that phases such as α-(Fe, Cr), M_2B, TiC, and M_7C_3 were formed in coatings with 10% B content, and TiB_2 phase was also detected in coatings with 20% and 30% boron content. In addition, it was determined that the volume fraction ratio of TiB_2 phase increased in the coating microstructures and it was synthesised as a rod-like structure. Accordingly, the microhardness values of the hardfacing coatings increased significantly. The highest microhardness found was 1045 $HV_{0.2}$ for the coating produced from 30B-Ti composition, which is about 4.5 times higher than the base steel (234 $HV_{0.2}$).

Keywords: In situ, TiC-TiB_2, Hardfacing, Surface alloying, Hardness, Wear

*Sorumlu yazar / Corresponding author: bkilinc@subu.edu.tr
Bu makaleye atıf yapmak için /To cite this article

Kılınç, B. (2024). The Influence of B Content on the Microstructure and Hardness of in Situ Formed TiC-TiB_2 Reinforced Fe-Based Hardfacing Coatings. Journal of Materials and Mechatronics: A (JournalMM), 5(2), 327-340.

1. INTRODUCTION

Hardfacing is a powerful and inexpensive deposition method used to repair worn parts or to improve their wear properties. This method is widely used in heavy industries and extends the service life of components by improving their wear, corrosion and impact resistance (Ahn, 2013; Durmuş et al., 2018; Variables & Works, 2023). Various welding methods are used for hardfacing. Among these methods, plasma transfer arc (PTA) welding (Brezinová et al., 2021; D'Oliveira et al., 2006; Huang et al., 2022), laser cladding (Hu et al., 2024), gas metal arc welding (GMAW) (Pawlik et al., 2023) and tungsten inert gas (TIG) welding (Jozwik et al., 2018) etc. are the most common ones. Among these methods, hardfacing coatings made by TIG welding are more preferred due to the low cost of equipment (Kumar & Das, 2022; Lin et al., 2010). In the TIG method, an arc is created between the tungsten electrode and the workpiece, and the resulting high heat melts the layer previously placed on the steel surface. Thus, by melting the coating powder on the steel substrate, coating layers with high hardness and high wear properties are obtained. (Buytoz & Ulutan, 2006). For this reason, many researchers have successfully used the TIG method to produce a hard and wear-resistant coating in their work.

In composite coatings, the mixture of a highly ductile metal matrix and hard reinforcement phases improves wear and hardness properties. To produce these composites, firstly, high hardness ceramic particles are directly reinforced. In the second method, various reinforcement phases (TiB, TiB_2 and TiC, etc.) are formed by in-situ synthesis in a melt pool (Weng et al., 2022). TiB_2 and TiC ceramics are the most widely used ceramics to improve the mechanical performance of coatings due to their great features such as high melting point, high hardness, and high thermal stability (Chen et al., 2022; Gupta et al., 2022). Wang et al (Wang et al., 2008) produced composite hardfacing coatings reinforced with in situ TiC and TiB_2 particles by forming different mixtures of Fe, Ti and B_4C powders by argon arc welding. Zhang et al. (Zhang et al., 2017) fabricated Fe-based composite coatings reinforced with Fe-Ti-Cr-B-C particles by laser cladding technique. They prepared FeTi30 (Ti about 30 wt%), B_4C (90 wt%) and iron powders in a mixed ratio as precursor powders. The effects of ferrochrome (FeCr) addition to these powders on the microstructure and mechanical properties of the coatings were investigated. Tang (Tang, 2016), deposited TiC-TiB_2 composite coating on the surface of 40Cr steel by electrical discharge hardening with a TiC-TiB_2 composite rod as an electrode. The structure, phase compositions, hardness and wear properties of the composite coating were investigated. The composite rod used for the coating process was prepared by self-propagating high-temperature synthesis of Ti and B_4C powders. In the literature, the use of Ti and B_4C powders to produce in situ TiC-TiB_2 reinforced hardfacing coatings is common, but the use of ferroalloys is limited.

In this research, ferrous-boron, ferrous-chromium and ferrous-titanium were used as coating powders to produce TiC-TiB_2 reinforced Fe based hardfacing coating. The use of such ferroalloys as coating powders significantly reduces the cost of the coating material and also lowers the melting point of the coating material through eutectic reactions (Du et al., 2008). In this research, Fe-Cr-Ti-(C,B) based coatings with three different boron contents were deposited on low carbon steel surface by TIG welding method. The phase constituents, microstructure and hardness properties of the produced hardfacing coatings were systematically investigated.

2. MATERIALS AND METHODS

2.1 Materials

The steel substrate was first cut in dimensions of 30 mm × 80 mm × 10 mm and then grooved on its surfaces with a depth of 2 mm and a width of 10 mm on a milling machine. The surfaces of the prepared steel substrates to be subjected to the coating process were cleaned from dirt and oil.

Table 1. Chemical composition of the DIN St37 steel (wt.%)

C	Mn	S	P	Fe
0.22	1.5	0.03	0.033	Bal.

Ferrous-boron, ferrous-titanium, ferrous-chromium, and iron powder were used for the hardfacing process. The compositions of the ferroalloy powders used for the formation of Fe-Cr-Ti-(B,C) based hardfacing coatings are given in Table 2. Ferroalloys in rock form were first crushed. After crushing, they were ground in a Retch ring mill with a sieve size of 75 μm.

Table 2. Composition of used ferroalloys (wt.%)

Ferro-alloys	Fe	B	Ti	Cr	C	Al
Ferrous-boron	81.82	18.1	-	-	0.19	-
Ferrous-chromium	33.35	-	-	60	0.15	1.5
Ferrous-titanium	25.2	-	70.95	-	0.13	3.96
Pure iron	99.98	-	-	-	-	-

Iron powder, which was supplied in powder form, was directly sieved to a sieve size of 75 μm. A pre-written excel programmed was used to atomically determine the hardfacing compositions at the desired ratios. With the help of this program, the ferroalloys whose weight ratios are given in Table 2 were first converted into atomic ratios. Then, by entering the desired atomic values, the required amount of each ferroalloy by weight was calculated. Finally, the powders were weighed and mixed on a precision balance according to the composition ratios given in Table 3. Thus, the desired alloy ratios for hardfacing were formed.

Table 3. Atomic ratios of the compositions prepared for hardfacing (at.%)

Metal Alloys	Fe	Cr	Ti	C	B
10B-Ti	55	15	15	5	10
20B-Ti	45	15	15	5	20
30B-Ti	35	15	15	5	30

2.2 Hardfacing Process

The powders prepared in three different compositions were subjected to grinding and mixing process in MSE TECH brand mill at 200 rpm for 1 hour. In the mixing process, the powder/ball ratio was selected as 1/3. Steel balls with a diameter of 7 mm were used for mixing. The containers and balls were thoroughly cleaned with pure alcohol before mixing. The powder mixtures were mixed with potassium silicate (K_2O_3Si) with the help of a metal rod until a paste consistency was obtained. The powder mixture was plastered one by one to fill the channels in the substrate materials. The resulting sample was dried in the open air for 24 hours and then heated in an oven at 250^oC for 2 hours.

The powders dried in channels on the steel substrate surface were melted by tungsten inert gas (TIG) welding method for hardfacing. Hardfacing operations were carried out using a Magmaweld ID 220T AC/DC Pulse brand TIG inverter welding machine with 160 A welding current, 20 V welding voltage, 12 L/min argon (99.9%) flow rate and Type W-2 pct ThO2 tungsten electrode. The coated specimens were then cooled in an open atmosphere and subjected to sandblasting to remove the oxide layer and slag formed during coating.

2.3 Metallographic Study

The samples coated by TIG process were cut perpendicular to the welding direction and bakelite was taken for microstructure examinations. The specimens were first subjected to sanding process for microstructure investigations. They were then polished with 1 μm Al2O3 paste and etched with 3% Nital solution. SEM-EDS examinations of the Fe-Cr-Ti-(C, B) based alloy formed on the surface were carried out with JEOL-JSM-6060 scanning electron microscope.

Phase analyses of the samples in which Fe-Cr-Ti-(C, B) based alloys were produced on their surfaces were carried out by using RIGAKU D/MAX/2200/PC brand x-ray diffractometer. CuKα (λ= 1,5408 A°) radiation was used during the analyses.

The microhardness measurements of the produced samples were carried out using FutureTech FM700 microhardness tester under 200 g load from the surfaces prepared for microstructure investigations. Measurements were made with a Vickers tool ($HV_{0.2}$) from the substrate to the surface at 0.2 mm intervals from three different areas as row hardness and the arithmetic mean was calculated.

3. RESULTS AND DISCUSSION

3.1 Microstructural and Phase Analysis

Figure 1 shows the SEM microstructure image of the cross-sectional area of the 30B-Ti sample coated on the DIN St37 steel surface. It can be seen that the hardfacing produced formed a metallurgical bond with the steel substrate and did not contain pores and any microscopic cracks. From the microstructure images, it is observed that there is a harmonious transition between the hardfacing and the substrate material, and a homogeneous coating structure is formed. In addition, the substrate, interface (fusion line), transition zone and coating layer can be clearly distinguished. In the hardfacing process performed by TIG welding, dilution of the coating layer may occur due to some melting of the substrate.

In this layer, called the transition zone in Figure 1, there is more iron content than the hardfacing coating layer. Therefore, the black rod-like (TiB_2) structures seen in the upper layers are not seen in this region. This is a result of solidification rate changes that are much higher in the upper regions of the coating layer. The solidification rate (R) from the fusion line (interface) to the coating surface increased and at the same time the temperature gradient (G) decreased. Therefore, this transition zone consists of planar growth, cellular and coaxial dendrite growth (Hajihashemi et al., 2015).

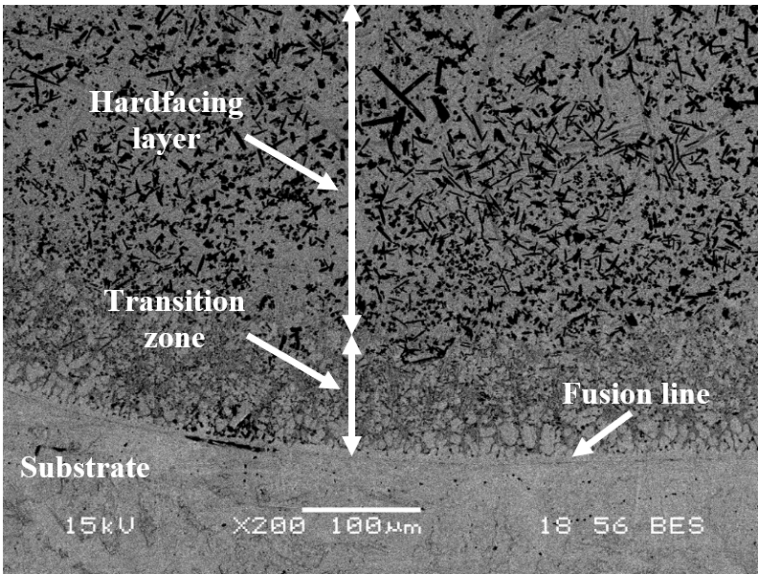

Figure 1. Cross-section of 30B-Ti sample

Figure 2 shows the XRD patterns of hardfacing coatings. As a result of XRD analyses, α-(Fe,Cr), M_2B (M= Fe,Cr), TiC and M_7C_3 phases were detected in the coating containing 10% B. In the coatings with 20% and 30% B content, the presence of TiB_2 phase was determined together with the above phases. Zhang et al. investigated the effect of Cr element in Fe-Cr-Ti-(C,B) based coatings and reported the presence of similar phases (Zhang et al., 2017).

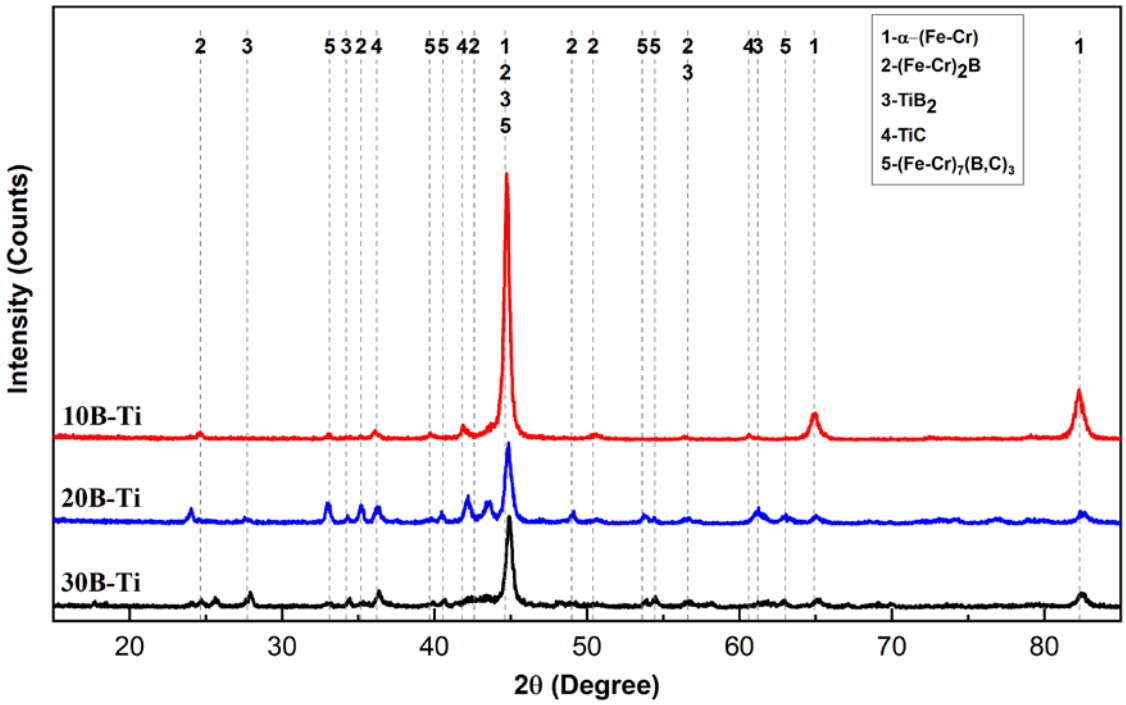

Figure 2. X-ray analysis patterns of hardfacing coatings

Figure 3 shows the SEM images, EDS, and MAP analyses of the 10B-Ti sample with an atomic boron content of 10%. SEM images show that the produced coating layer exhibits a hypoeutectic solidification. It is seen that Ti and C elements are dense in the EDS number 1 taken from the equiaxed dark regions distributed in the coating microstructure and in the MAP analysis given in Figure 3(i and j). In addition, the presence of TiC phase in this coating was found in the X-ray analysis given in

Figure 2, supporting that these regions consist of TiC phase. In the EDS analysis number 2 taken from the light grey regions in the coating microstructure, signals of Fe and Cr elements were obtained. The same situation is also observed in MAP analysis and these regions are thought to be the hypoeutectic α-(Fe,Cr) phase. In the EDS analysis number 3 taken from the eutectic region of the coating, Fe and Cr peaks were quite intense, but very few B and C peaks were measured (Figure 3 (e)). Again, when the elemental distribution maps of the eutectic region were analysed, Cr and Fe were found to be intense, and C and B elements were also detected in these regions, albeit slightly (Figure 3 (f-k).

As a result of the X-ray analysis given in Figure 2, it was determined that M_2B and M_7C_3 (M= Fe,Cr) phases were also present in this composition. Therefore, it is thought that the eutectic structure consists of α-Fe+M_2B and/or M_7C_3 phases.

Figure 4 shows the SEM images, EDS, and MAP analyses of the 20B-Ti sample in which the boron ratio atomically increases to 20%. SEM images show that the coating microstructure consists of complex structures (Figure 4 (a and b)). During coating on the steel surface by TIG welding method, the melt pool of this compound is rich in B and it is easier to form TiB_2 phase. For this reason, it is thought that the first structure formed in the melt pool due to cooling is the TiB_2 phase. It is expected that the TiC phase will be formed in the continuation of solidification. In their study, Weng et al. reported that thin TiB_2 lamellae were first formed in the melt pool and then the TiC phase nucleated on these lamellae by heterogeneous nucleation (Weng et al., 2022). SEM images, EDS and MAP analyses given in Figure 4 show that TiC phase is present around the polygonal TiB_2 structures.

As a result of the EDS analysis number 2 taken from the black colored polygonal regions shown in Figure 4 (d) and the MAP analysis given in Figure 4 (j and l), it is seen that these structures are rich in Ti and B elements. When evaluated with the X-ray analysis given in Figure 2, it can be assumed that these structures consist of TiB_2 phase. As a result of the EDS signal number 4 taken from the dark grey colored coaxial structures and the MAP analysis given in Figure 4 (j and k), it is clearly seen that these regions are rich in Ti and C elements. When compared with XRD results, it is possible to say that these regions consist of TiC phase.

EDS analyses of the light white regions in the coating layer showed that they are rich in iron, and also contain Cr and very little Ti elements (Figure 4 (c)). According to MAP analyses and XRD results, it was determined that these structures consist of α-(Fe,Cr). In addition, light grey long strip-like structures were observed in the microstructure in SEM images. Gramajo et al. identified these structures as $M_7(B,C)_3$ (Gramajo et al., 2020). In addition, it was determined by EDS analysis number 3 that these structures are rich in Cr and Fe elements. According to XRD analyses, these structures are thought to be $(Fe,Cr)_7$ $(B,C)_3$.

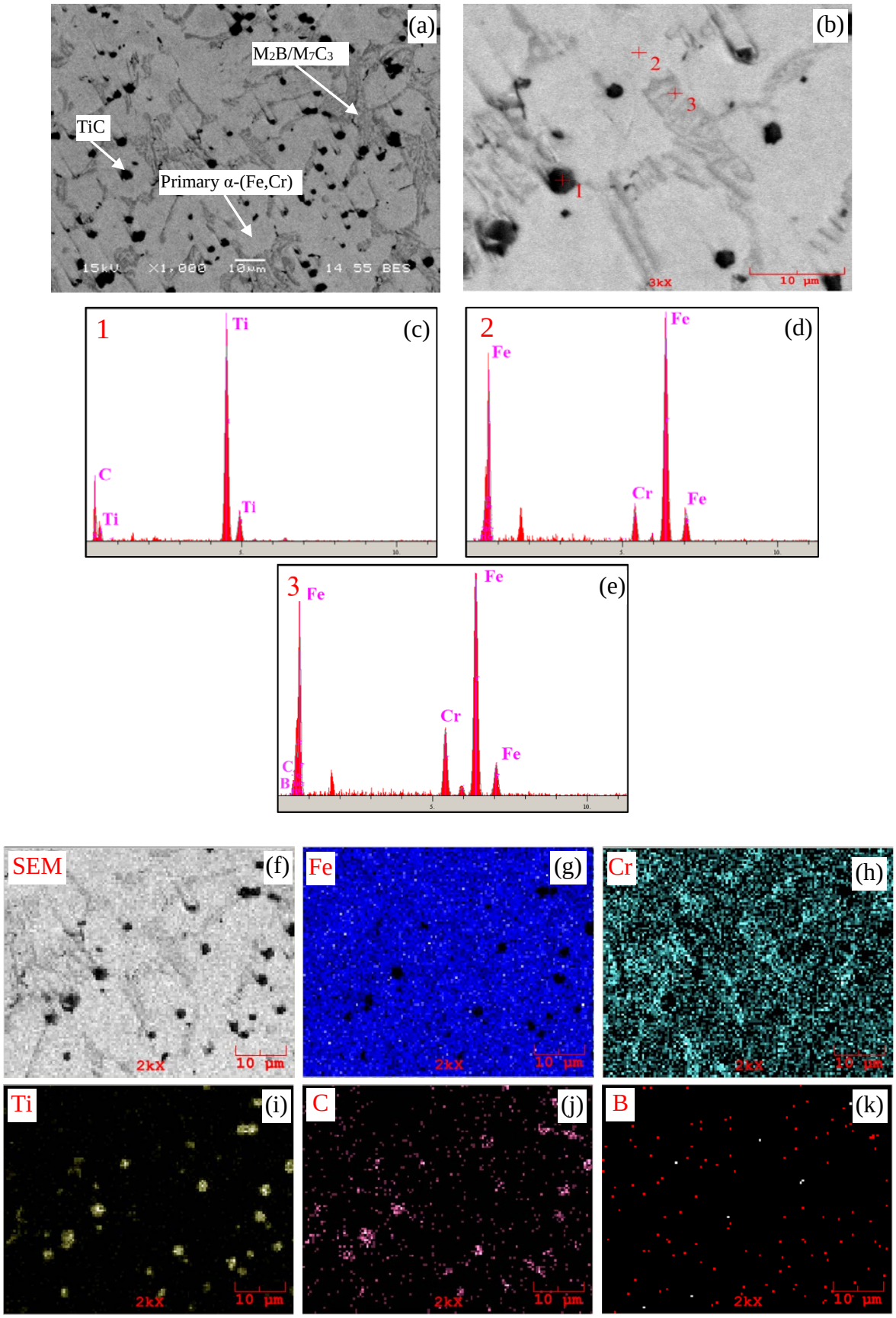

Figure 3. SEM images (a and b), EDS analyses (c-e) and elemental distribution maps (f-k) of 10B-Ti sample

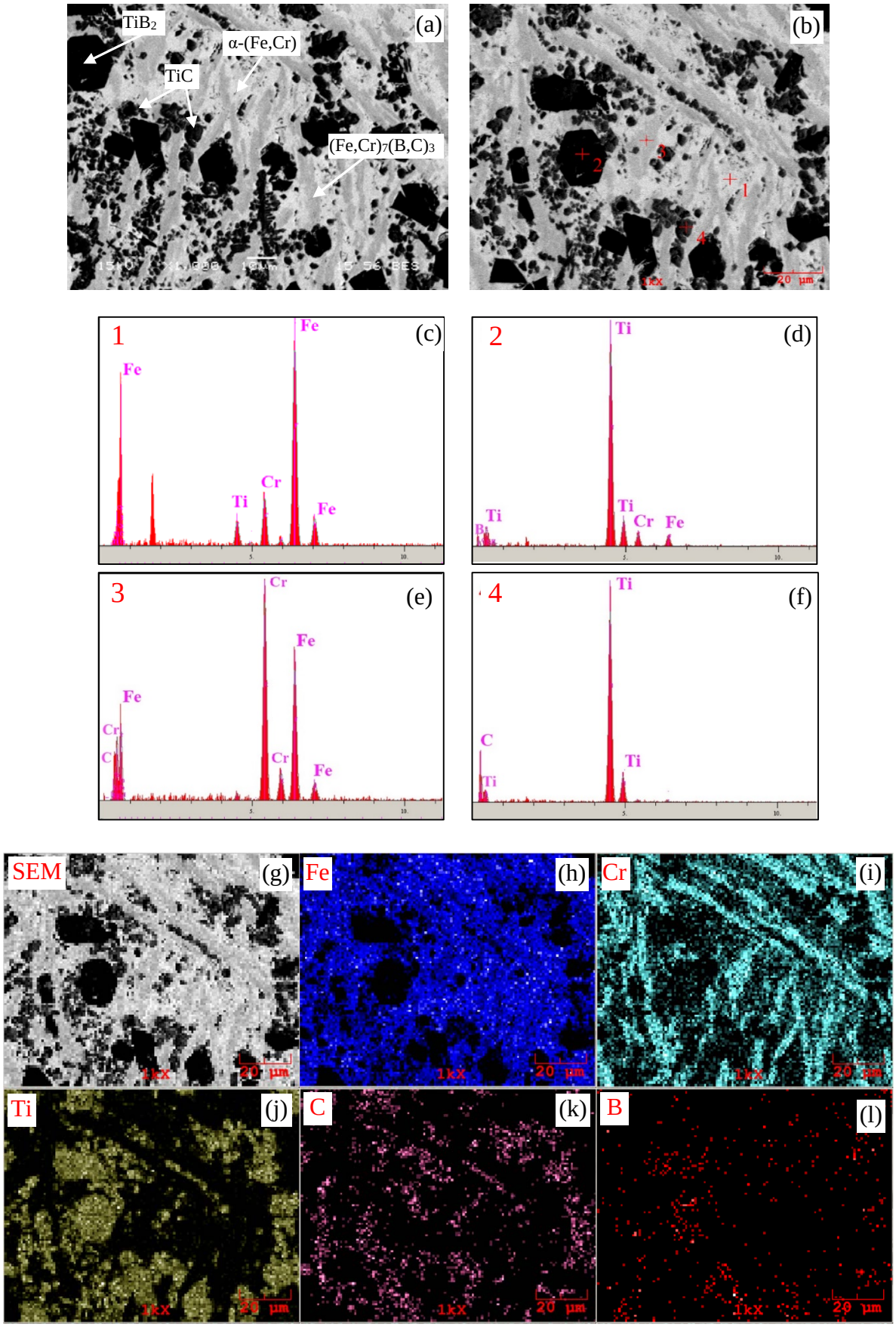

Figure 4. SEM images (a and b), EDS analyses (c-f) and elemental distribution maps (g-l) of 20B-Ti sample

SEM images, EDS and MAP analyses of 30B-Ti sample are given in Figure 5. This sample also exhibits a hypereutectic microstructure like the 20B-Ti sample. However, the black colored polygonal structures seen in the 20B-Ti sample are seen as black colored rod-like and long sharp-cornered phase formations in the 30B-Ti sample. It has been reported that increasing titanium and boron concentrations in the alloy system are effective in the formation of these structures. (Kaptanoglu & Eroglu, 2017; Kocaman et al., 2022).

As a result of the EDS and MAP analyses given in Figure 5, it was determined that these structures are also rich in Ti and B elements. Therefore, it can be said that these structures are TiB_2 phase. Ti and C elements were detected in the dark grey coloured equiaxed structures around the TiB_2 phase and in the matrix. As a result of the x-ray analysis given in Figure 2, these structures were determined to be TiC. A similar microstructure formation was shown in the study by Zhang et al. Two different types of coloured particles were identified in the coating layer. One is grey particles forming the cubic or flower-like TiC phase and the other is black particles forming the block-like TiB_2 phase (Zhang et al., 2020). Similar to our study, TiC phases are located in the matrix and around TiB_2 phases.

It can be said that the first structure to form during the solidification of the 30B-Ti sample formed on the steel surface is the TiB_2 phase. In the continuation of solidification, TiC phase was formed and clustered around the TiB_2 phase. As explained above, TiC phase will nucleate heterogeneously on thin TiB_2 lamellas solidified in the coating bath. With the nucleation and subsequent growth of the TiC phase on the TiB_2 lamellae, the B element dissociates at the liquid-solid interface. With the dissociated B element, TiB_2 is ready to nucleate and grow again. Therefore, the TiB_2 phase continues to grow by two-dimensional nucleation and lateral spreading (Li et al., 2013). Weng et al. stated that due to the rapid cooling and rapid solidification occurring in the coating layer, the lamellar structures formed from the TiB_2 phase in this layer will not transform into hierarchical tower-like and dendritic morphologies, but will remain in plate-like morphology (Weng et al., 2022). When the SEM images and EDS analyses of the 30B-Ti sample given in Figure 5 are examined, it is seen that the microstructure formation is in accordance with the above description.

As in the 20B-Ti sample, Cr and Fe elements are present in the light-colored regions of this sample. Therefore, it is possible to say that in addition to the iron-rich α-(Fe,Cr) phase, very little M_2B phase is also present in the structure. In this coating, the light grey long rod $(Fe,Cr)_7(B,C)_3$ phase is also present.

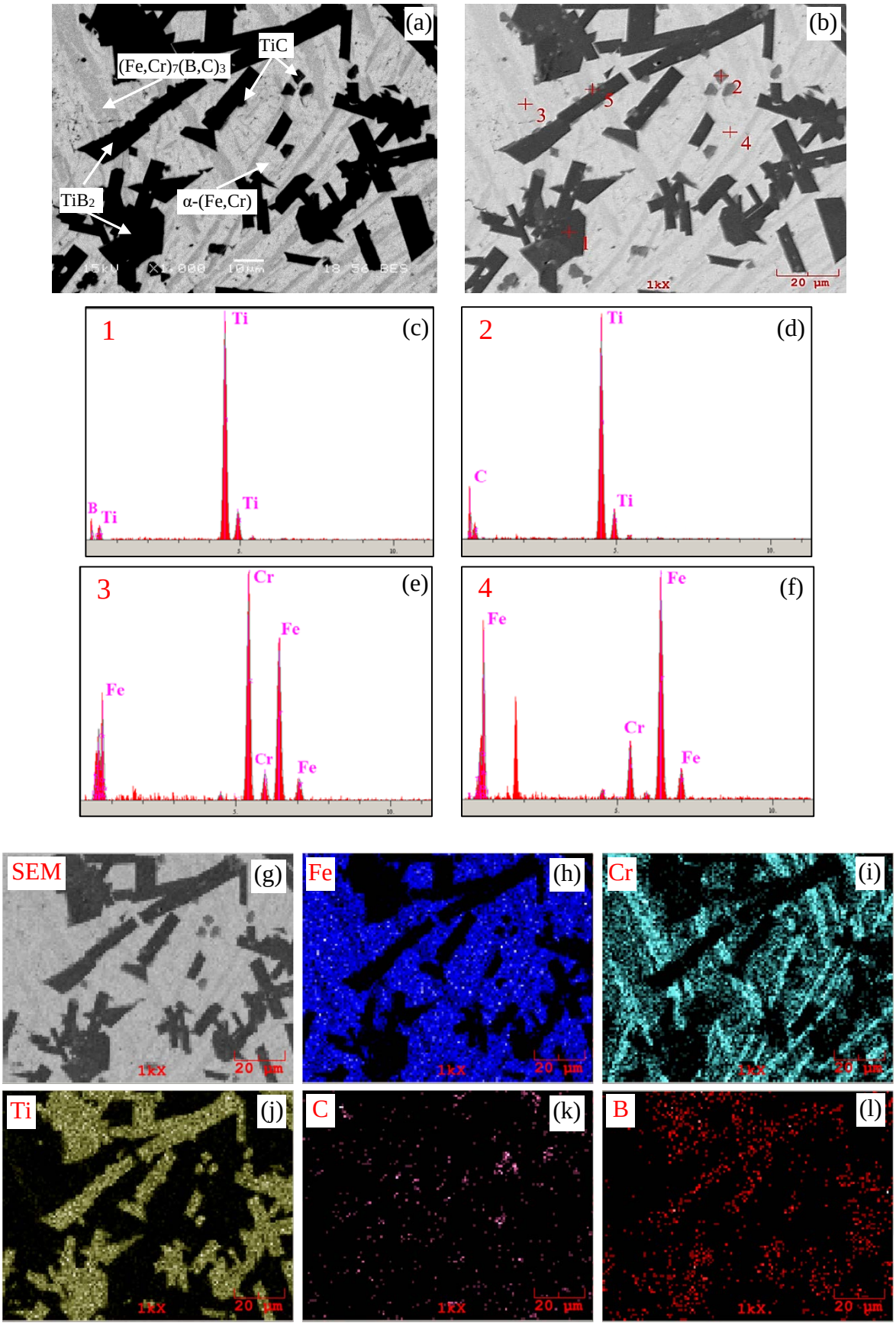

Figure 5. SEM images (a and b), EDS analyses (c-f) and elemental distribution maps (g-l) of 30B-Ti sample

3.2 Hardness

Figure 6 shows the microhardness values of the coated samples measured at 0.2 mm intervals from the substrate to the coating surface. In such composite coatings, the microhardness values are strongly influenced by the volume fraction of phases with high hardness values, such as borides and carbides, present in the structure as reinforcing phases (Amushahi et al., 2010; Du et al., 2008; Venkatesh et al., 2015). When the graph is examined, it is seen that the microhardness increases as the B content in the coating increases.

When the B content was increased from 10at.% to 30 at.%, the hardness of the coating increased from an average of 544 to 1045 $HV_{0.2}$. The maximum hardness was determined in the 30B-Ti sample with 30 at.% B content, which is approximately 4.5 times higher than the microhardness value of DIN St37 steel (234$HV_{0.2}$).

As determined in the microstructure examinations, the 10B-Ti sample with the lowest B ratio had a hypoeutectic microstructure and the hard particle phase TiC was homogeneously distributed in the structure. However, the volume fraction of the hard particle reinforcement phase in this sample was very low compared to the matrix phase. In addition, eutectic structures with M_2B and $(Fe,Cr)_7(B,C)_3$ phases were also observed to be present at lower rates compared to other samples. In the 20B-Ti and 30B-Ti samples, where the B ratio increased, a microstructure hypereutectic was detected. In these samples, TiB_2, which is a hard particle reinforcement phase, was observed to increase significantly in the microstructure. Therefore, the increase in the B ratio in the coating greatly affected the microstructure and significantly increased the microhardness of the hardfacing.

When the graph given in Figure 6 is analyzed, it is determined that there are fluctuations in microhardness values. It is known that these fluctuations in hardness results are due to hard particle reinforcement structures such as TiC and TiB_2 in the coating microstructure (Kocaman et al., 2020; Kumar & Das, 2022). It is also observed that the microhardness values for all specimens increase slightly from the substrate to the coating layer. Microhardness values depend on the concentration and shape of the coating layer as well as the distribution of the coating microstructure (Kumar & Das, 2022). Hardness values are expected to be lower in the coating layer close to the substrate due to the dilution effect. As you move to the upper layers of the coating layer, the volume fractions of hard phases such as TiB_2 and TiC increase, which leads to an increase in microhardness.

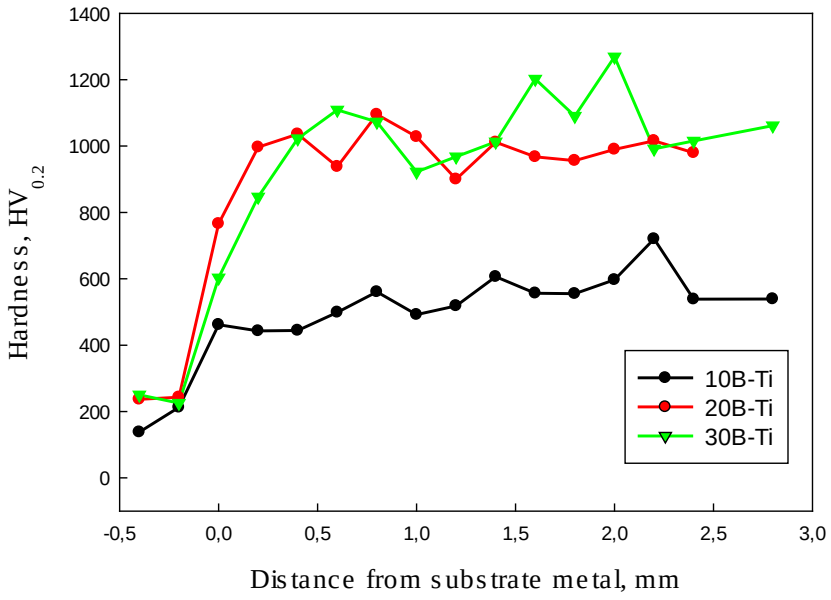

Figure 6. Microhardness values of Fe-Cr-Ti-(C, B) based hardfacing

4. CONCLUSION

This study presents the effects of B content on the microstructural changes and hardness of Fe-based in-situ TiC-TiB_2 hardfacing coatings. The main conclusions are as follows:

- Fe-Cr-Ti-(C,B) based coatings were successfully produced by TIG method and the coatings were found to be compatible with the substrate. No porosity and microscopic cracks were observed in the coating layer. The hardfacing layer, transition zone and interface (fusion line) were determined by microstructure images.
- Boron content significantly affected the microstructure of hardfacing coatings. The coating layer with a B content of 10% had a hypoeutectic microstructure. In this sample, a homogeneously distributed equiaxed dark colored TiC phase and α- (Fe, Cr) phase were detected. In eutectic regions, α-Fe+M_2B and/or M_7C_3 phases were found. The proportion of black colored polygonal TiB_2 phases was intense in the coating microstructure where the B ratio increased to 20%. In addition, $(Fe, Cr)_7(B,C)_3$ phases were also detected in the structure as long strips. Polygonal TiB_2 structures were observed as black colored rod-like and long sharp-cornered phases in the coating with 30% B content, which exhibited eutectic microstructure. TiC phase was detected around the TiB_2 phase and in the matrix. In this coating, the light grey long rod $(Fe, Cr)_7(B,C)_3$ phase is also present in this coating together with the M_2B phase.
- It was observed that the microhardness of Fe-Cr-Ti-(C,B) hardfacing coatings increased as the amount of B increased. The highest microhardness was found in 30B-Ti sample with 1045 $HV_{0.2}$. It was also observed that the microhardness values increased from the substrate to the surface of the coating layer.

5. ACKNOWLEDGEMENTS

This study did not receive funding support from any institution or organization.

6. CONFLICT OF INTEREST

Author approves that to the best of their knowledge, there is not any conflict of interest or common interest with an institution/organization or a person that may affect the review process of the paper.

7. AUTHOR CONTRIBUTION

Bülent KILINÇ has the full responsibility of the paper about determining the concept of the research, data collection, data analysis and interpretation of the results, preparation of the manuscript and critical analysis of the intellectual content with the final approval.

8. REFERENCES

Azzi M., Paquette M., Szpunar J.A., Klemberg-Sapieha J.E., Martinu L., Tribocorrosion behaviour of DLC-coated 316L stainless steel. Wear 267 (5-8), 860-866, 2009.

Ahn D. G., Hardfacing technologies for improvement of wear characteristics of hot working tools: A review. International Journal of Precision Engineering and Manufacturing, 14(7), 1271-1283, 2013.

Amushahi M. H., Ashrafizadeh F., Shamanian M., Characterization of boride-rich hardfacing on carbon steel by arc spray and GMAW processes. Surface and Coatings Technology, 204(16-17), 2723–2728, 2010.

Brezinová J., Viňáš J., Guzanová A., Živčák J., Brezina J., Sailer H., Vojtko M., Džupon M., Volkov A., Kolařík L., Rohan P., Puchý V., Selected properties of hardfacing layers created by pta technology. Metals, 11(1), 1-20, 2021.

Buytoz S., Ulutan M., In situ synthesis of SiC reinforced MMC surface on AISI 304 stainless steel by TIG surface alloying. Surface and Coatings Technology, 200, 3698-3704, 2006.

Chen L., Yu T., Guan C., Zhao Y., Microstructure and properties of metal parts remanufactured by laser cladding TiC and TiB2 reinforced Fe-based coatings. Ceramics International, 48(10), 14127-14140, 2022.

D'Oliveira A. S. C. M., Paredes R. S. C., Santos R. L. C., Pulsed current plasma transferred arc hardfacing. Journal of Materials Processing Technology, 171(2), 167-174, 2006.

Du B., Zou Z., Wang X., Qu S., Laser cladding of in situ TiB2 /Fe composite coating on steel. Applied Surface Science, 254(20), 6489-6494, 2008.

Durmuş H., Çömez N., Gül C., Yurddaşkal, M., Yurddaşkal, M., Wear performance of Fe-Cr-C-B hardfacing coatings: Dry sand/rubber wheel test and ball-on-disc test. International Journal of Refractory Metals and Hard Materials, 77(June), 37-43, 2018.

Gramajo J., Gualco A., Svoboda H., Study of the welding procedure in nanostructured super-hard Fe-(Cr, Mo, W) - (C, B) hardfacing. International Journal of Refractory Metals and Hard Materials, 88(December 2019), 1-6, 2020.

Gupta N. K., Pyla K. R., Debta M. K., Masanta M., Performance evaluation of TIG cladded in-situ TiC-TiB2 composite coating fabricated on AISI304 stainless steel. Materials Today: Proceedings, 62(P10), 5956-5961, 2022.

Hajihashemi M., Shamanian M., Azimi G., Physical, Mechanical, and Dry Sliding Wear Properties of Fe-Cr-W-C Hardfacing Alloys Under Different Tungsten Addition. Metallurgical and Materials Transactions B, 46, 919-927, 2015.

Hu Z., Zhang, D., Wu D., Zheng, X., Sun J., Geng P., Ma N., Enhanced mechanical properties of Fe-based hardfacing alloy with Al additions fabricated by laser cladding. Surface and Coatings Technology, 478(January), 130447, 2024.

Huang Y., Huang J., Yu X., Yu S., Fan D., Microstructure characterization and texture evolution of Ti-6Al-4V cladding layer fabricated by alterative current assisted TIG. Surface and Coatings Technology, 431, 128014, 2022.

Jozwik J., Dziedzic K., Usydus I., Ostrowski D., & Krolczyk G. M., Assessment of internal defects of hardfacing coatings in regeneration of machine parts. Journal of Central South University, 25(5), 1144-1153, 2018.

Kaptanoglu M., Eroglu M., Microstructure and wear of iron-based hardfacings reinforced with in-situ synthesized TiB2 particles. Kovove Materialy, 55(2), 123-131, 2017.

Kocaman E., Kılınç B., Şen Ş., Şen U., Effect of chromium content on Fe(18-x)CrxB2(X=3,4,5) hardfacing electrode on microstructure, abrasion and corrosion behavior. Journal of the Faculty of Engineering and Architecture of Gazi University, 36(1), 177-190, 2020.

Kocaman E., Kılınç B., Şen Ş., Şen U., In-situ TiB2 and Fe2Ti intermetallic assisted hard coatings by Fe-Ti-B based hardfacing electrodes. Journal of Alloys and Compounds, 900, 163478, 2022.

Kumar S., Das A. K., Wear resistance and hardness properties of TiB2– Fe coating developed on AISI 1020 steel by tungsten inert gas (TIG) cladding. Ceramics International, 48(20), 30052-30065, 2022.

Li P., Wu Y., Liu X., Controlled synthesis of different morphologies of TiB2 microcrystals by aluminum melt reaction method. Materials Research Bulletin, 48(6), 2044-2048, 2013.

Lin C. M., Chang C. M., Chen J. H., Hsieh C. C., Wu W., Microstructure and wear characteristics of high-carbon Cr-based alloy claddings formed by gas tungsten arc welding (GTAW). Surface and Coatings Technology, 205(7), 2590-2596, 2010.

Pawlik J., Bembenek M., Góral T., Cieślik J., Krawczyk J., Łukaszek-Sołek A., Śleboda T., Frocisz Ł., On the Influence of Heat Input on Ni-WC GMAW Hardfaced Coating Properties. Materials, 16(11), 2023.

Tang J., Mechanical and tribological properties of the TiC-TiB2 composite coating deposited on 40Cr-steel by electro spark deposition. Applied Surface Science, 365, 202-208, 2016.

Variables P., Works F., A Review on Hardfacing, Process Variables, Challenges, and Future Works. Metals, 13 (1512), 1-37, 2023.

Venkatesh B., Sriker K., Prabhakar V. S. V., Wear Characteristics of Hardfacing Alloys: State-of-the-art. Procedia Materials Science, 10(Cnt 2014), 527-532, 2015.

Wang Z. T., Zhou X. H., Zhao G. G., Microstructure and formation mechanism of in-situ TiC-TiB2/Fe composite coating. Transactions of Nonferrous Metals Society of China (English Edition), 18(50075085), 831-835, 2008.

Weng F., Yu H., Du X., Tian H., Chen C., In situ formed TiB2/TiC complex structure in laser-alloyed coatings with improved wear property. Ceramics International, 48(5), 7056-7062, 2022.

Zhang M., Qu K. L., Luo S. X., Liu S., Effect of Cr on the microstructure and properties of TiC-TiB2 particles reinforced Fe-based composite coatings. Surface and Coatings Technology, 316, 131-137, 2017.

Zhang M., Zhao G. L., Wang X. H., Liu S. S., Ying W. L., Microstructure evolution and properties of in-situ ceramic particles reinforced Fe-based composite coating produced by ultrasonic vibration assisted laser cladding processing. Surface and Coatings Technology, 403, 126445, 2020.